Beyond Topographic Mapping: Towards Functional-Anatomical Imaging with 124-Channel EEGs and 3-D MRIs

Alan Gevins,* Paul Brickett,* Bryan Costales,* Jian Le,* and Bryan Reutter*

Summary: A functional-anatomical brain scanner that has a temporal resolution of less than a hundred milliseconds is needed to measure the neural substrate of higher cognitive functions in healthy people and neurological and psychiatric patients. Electrophysiological techniques have the requisite temporal resolution but their potential spatial resolution has not been realized. Here we briefly review progress in increasing the spatial detail of scalp-recorded EEGs and in registering this functional information with anatomical models of a person's brain. We describe methods and systems for 124-channel EEGs and magnetic resonance image (MRI) modeling, and present first results of the integration of equivalent-dipole EEG models of somatosensory stimulation with 3-D MRI brain models.

Key words: EEG; EP; MRI; Functional neuroanatomy; Laplacian derivation; Deconvolutioin; Dipole localization, Topography; Computer systems; Signal processing.

Introduction

There are a number of techniques for monitoring brain function that are more or less noninvasive, including Positron Emission Tomography (PET), Single Photon Emission Computed Tomography (SPECT), Magnetic Resonance Imaging, (MRI) Electroencephalography (EEG) and Magnetoencephalography (MEG). Although the 3-Dimensional (3-D) anatomical imaging capabilities of EEG or MEG are not comparable to PET, SPECT or MRIs, EEGs and MEGs uniquely offer temporal resolution in the millisecond range. This particular capability is invaluable for studying seizure disorders and neurocognitive processes. With improving recording and analysis technologies, other valuable information that generations of clinicians and researchers over the past 60 years have believed was hidden in the EEG is becoming more accessible (see reviews in Lopes da Silva et al. 1986; Gevins and Remond 1987). Indeed, as technical capabilities have increased, so has the specificity of information extracted from EEGs, and the value of further developing methods to mine this hidden information is clearly mandated by the noninvasiveness and low cost of scalp EEG measurements for obtaining split-second information about brain function.

While spatial EEG features have often been difficult to discern in polygraph tracings, the recent availability of EEG color topographic maps has made appreciating them easy, even for the non-EEG specialist. The utility of the maps would be even greater if more spatial detail were available, and if the scalp EEG patterns could be registered with underlying brain anatomy. During the past 8 years, we have made some modest progress towards this end. We have improved and expanded our recording and analysis capabilities to accommodate 124 EEG channels, and have developed methods for reducing blur distortion of EEGs by the skull. We have implemented programs for processing magnetic resonance images, and we are developing a means of automatically constructing three-dimensional (3-D) models of a subject's brain. In tests of our method for registering EEGs and MRIs using somatosensory stimulation data, we obtained good results. Previous reports of prior stages

*EEG Systems Laboratory and SAM Technology, San Francisco, CA, USA.

Accepted for publication: June 24, 1990.

Acknowledgments: This work was supported by grants from agencies of the Federal government of the United States of America, including The National Institute of Neurological Diseases and Strokes, The National Institute of Mental Health, The Air Force Office of Scientific Research and The National Science Foundation. We gratefully acknowledge this support, as well as the efforts of our colleagues at the EEG Systems Laboratory, Drs. S. Bressler, B. Cutillo, and J. Illes, for their contributions to the research presented here.

Correspondence and reprint requests should be addressed to Alan Gevins, EEG Systems Laboratory, 51 Federal St., San Francisco, CA, USA, 94107.

Copyright © 1990 Human Sciences Press, Inc.

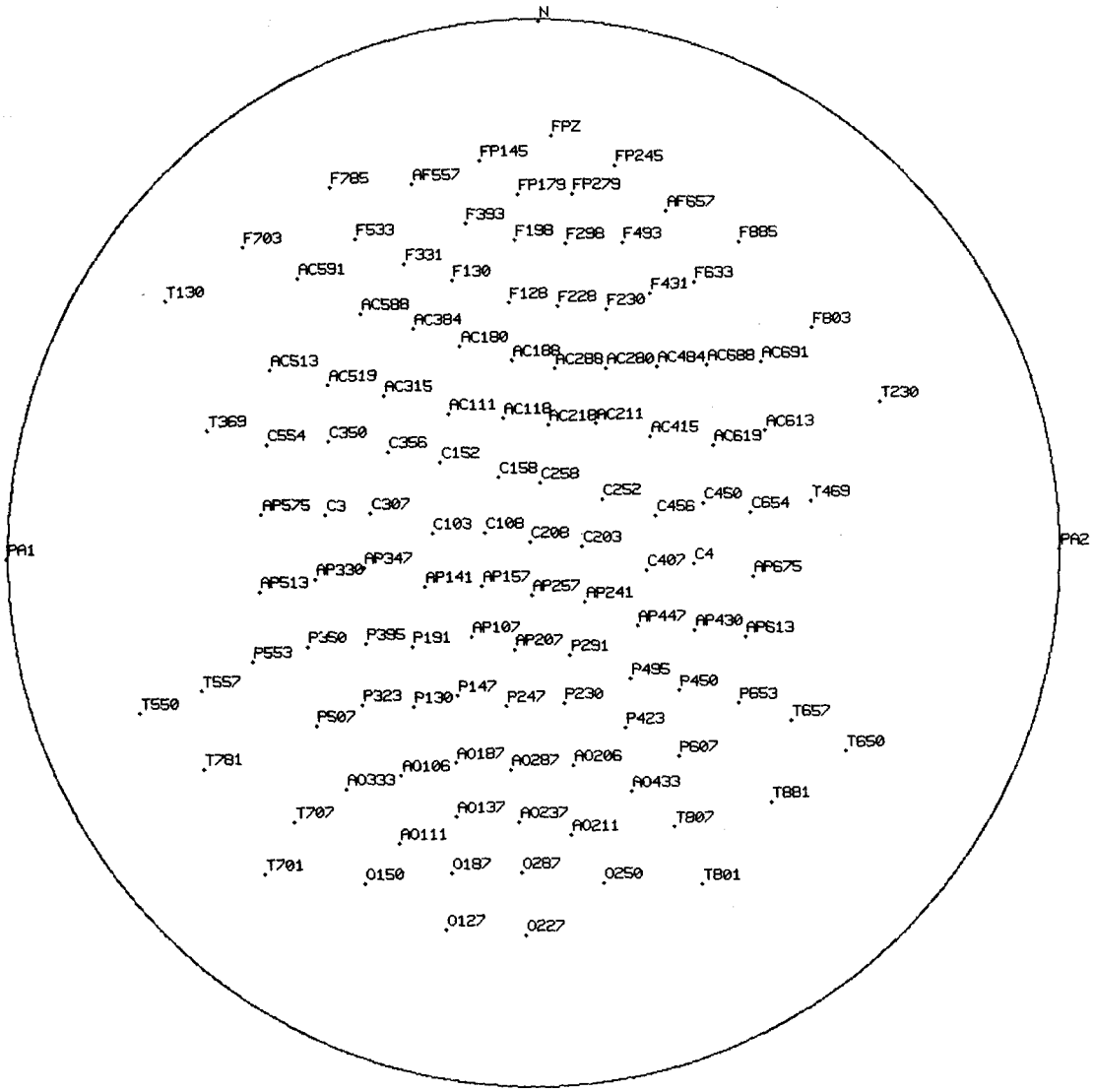

Figure 1: Diagram of 124-channel scalp montage. Electrode names are based on 10-20 system with additional letter prefixes and numerical suffixes (see text).

of progress in this regard have been published in Gevins (1987, 1988, 1989a,b).

EEG Recording Method

Extended 10-20 system

Several nomenclatures for defining electrode placements added to the original nineteen placements of the International 10-20 System (Jasper 1958) have been published (see Gevins 1988). Regardless of which nomenclature is used, the basic idea is that extra equidistant coronal rows are added between the original rows, and extra equidistant electrodes are added to fill in the spaces in each row. Our current 124-channel montage is shown in Figure 1. In the system we use, the letter "a" is prefixed to an existing 10-20 row name to indicate a position anterior to the existing one. For example, aO is anterior occipital, aP is anterior parietal, aC is anterior central and aF is anterior frontal. Two additional numbers appear after the location number (1-8) of the 10-20 positions. These two numbers (0-9) indicate the proportional distance to the next anterior and medial 10% electrode position, respectively. For example, an electrode halfway between P3 and aP1 would be named P355, while an electrode halfway between P3 and P1 would be named P305. With the original nineteen electrodes of the 10-20 System, the typical distance between electrodes on an average adult male head is about 6 cm; with 124 electrodes, the typical distance is 2.25 cm.

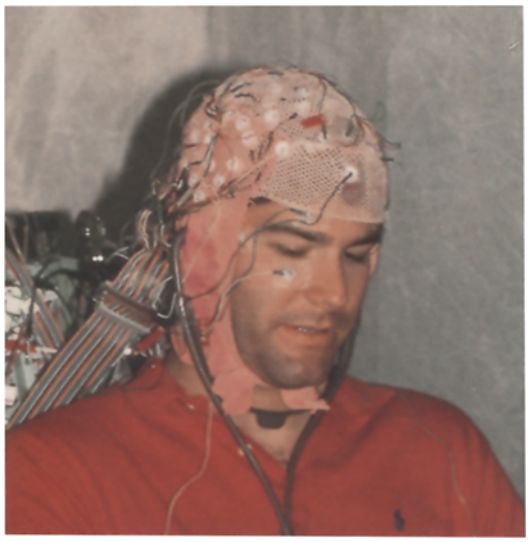

Figure 2: Subject wearing 124-channel EEG hat.

Electrode hat

In most routine clinical EEGs, electrodes are prepared and positioned on the head individually, while in some labs commercially available electrode caps with nineteen built-in electrodes are used. Extending the cap idea, we constructed one from a stretchable fabric, and populated it with 124 commercial tin-disk electrodes encased in plastic holders (Figure 2). The cap is positioned on the head by reference to the nasion, inion and preauricular notches. Individual recording sites are cleansed in the usual manner, and conducting gel is injected with a blunt needle through the top of each electrode. It takes a team of four research assistants about an hour to prepare a subject. While this is acceptable for infrequent research recordings, it is far too long and costly for routine use. We are developing a more efficient system for recording EEGs which we expect to greatly reduce application time.

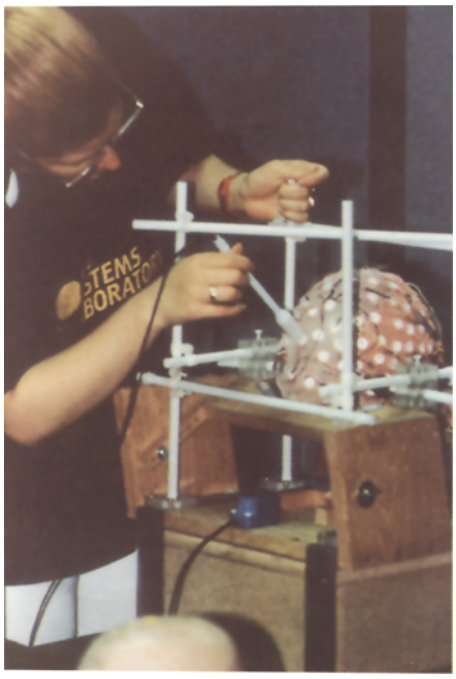

Figure 3: Measurement of electrode coordinates. The research assistant touches each electrode with a magnetic position sensor while the subject rests his head on a chin rest built into a head support which gently restricts head movement during the measurements. The 3-D coordinates of each electrode position are transmitted to the data collection computer.

Measuring electrode positions

Traditionally, individual electrodes are placed according to measurements taken with a tape measure. While this is sufficient when recording from 19 electrodes, greater precision is needed when many more electrodes are used and when one wishes to relate a recording position on the scalp to the underlying cortical anatomy. In our lab, the position of each electrode on a subject's head is measured with a probe that has coils for sensing the three-dimensional position of the probe tip with respect to a magnetic field source in the head support (Figure 3). Adjustable guides built into the head support hold the subject's head comfortably in place while the measurements are made. A menu-driven program is used to select electrodes to be measured and display the digitized position of each electrode on a two-dimensional projection display. Position measurement is accurate to better than 3mm [RMS]. Figure 4 shows the screen image of this program after all electrodes and some additional surface landmarks have been digitized.

Software system for data collection and analysis

Commercial EEG computer systems have vastly improved during the past few years, yet some important limitations still restrict their utility for researchers such as ourselves. This is a consequence of the fact that most systems have been designed for the clinical market where the central concern is to provide a series of fixed tests and measures. The most severe limitations are: (1) a way to implement new experimental protocols flexibly is rarely provided; (2) artifact detection and editing capabilities are too limited; (3) the system capacity for recording large numbers of channels and collecting and storing large databases is inadequate; (4) there are limited means of subdividing data to explore relationships between subsets of data and variations in a subject's responses or state; and (5) spatial analyses are underdeveloped, with

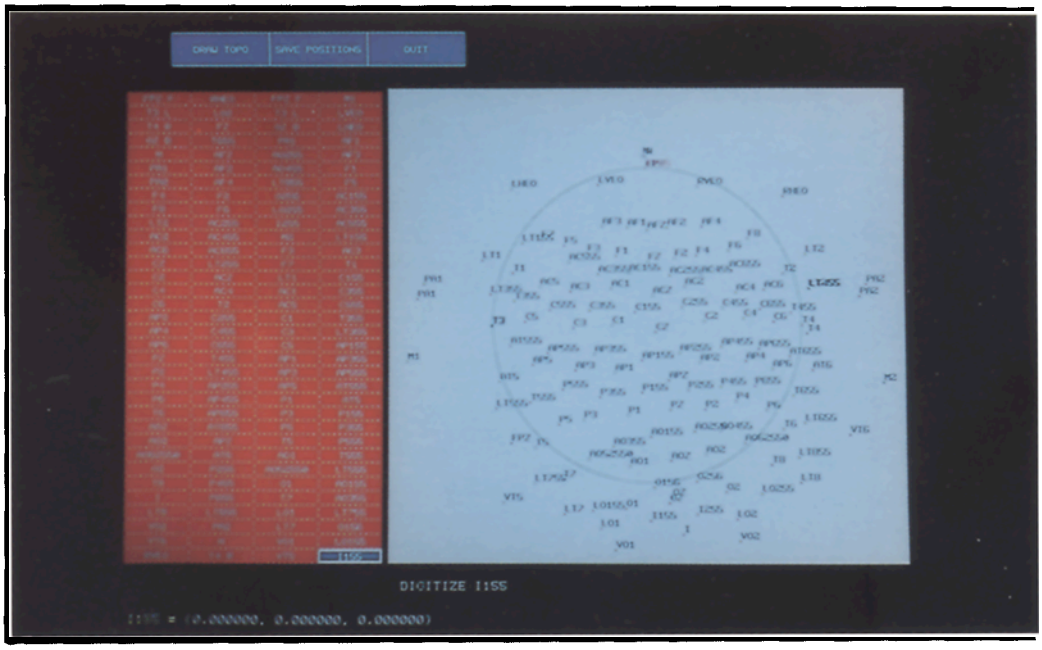

Figure 4: Graphic display of measured electrode positions. The menu at the left lists each of the electrode names. An initial three positions are used to determine the coordinate system, usually T3, T4 and Fpz. A circle, representing the head circumference, is then drawn around these three positions. Subsequent electrodes are shown in equidistant projection, with electrodes outside the circle representing locations lower than the circumference through T3, T4 and Fpz.

too few channels, a lack of spatial filters to reduce volume conduction distortion, a lack of cross-channel analyses (e.g., crosscovariance and crosspower, correlation and coherence), and the lack of means to investigate the relationship between neuroelectric data and cortical anatomy and physiology revealed by MRI and PET imaging technologies.

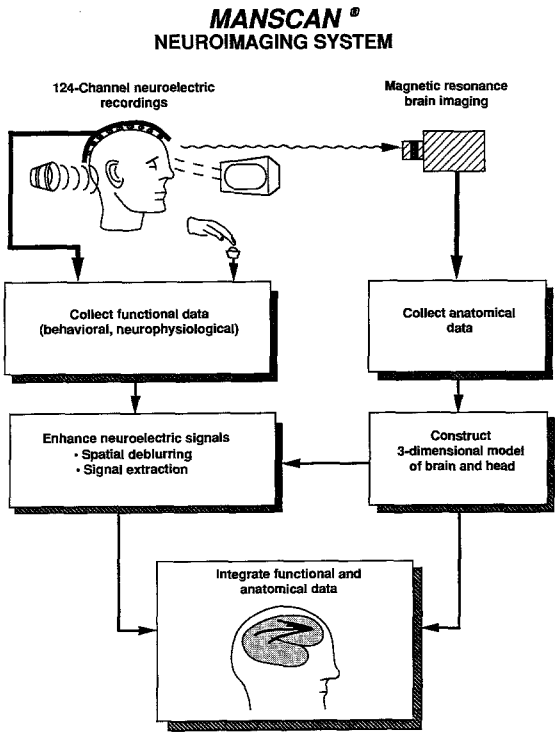

Figure 5: Manscan® functional-anatomical neuroimaging system.

The system we have been developing, now in its fifth generation, is aimed at overcoming these limitations (Gevins and Yeager 1972; Gevins et al. 1975, 1989; Gevins 1980, 1984, 1987; 1988) (Figure 5). This generation is distinguished from its predecessors architecturally by its self-decoding Data Description Language, network extensibility, and multi-window graphical user interface. As of May 1990, all the functions described in the following two paragraphs are fully operational.

1. Data Collection: In the fifth generation EEGSL system, two computers are used for data collection: a Concurrent 5700 and an IBM PC-compatible 386. The PC is used to present stimuli and gather behavioral response data from the subject, while the Concurrent collects physiological data and controls the PC. The Concurrent runs a real-time version of the UNIX operating system, while the PC runs the DOS operating system. We have written an experiment control software system which runs the two computers, presents a variety of visual, auditory and somatosensory stimuli according to flexible task protocols, and digitizes up to 256 channels of physiological data. Up to 128 EEG traces can be monitored in real time as data are collected. Most parameters of an experiment can be altered via a menu-

driven interactive display. A calibration module numerically adjusts the gain of all channels according to the magnitude of a calibration signal. Another module detects gross artifacts and color-codes contaminated data such as eye movements, gross head and body movements and bad electrode contacts on the operator's screen. Stimulus, behavioral and physiological data are stored on hard disk according to a self-decoding Data Description Language, and archived to magnetic tape. The data are immediately available to researchers at their desks using either remote terminals, or SUN workstations via Ethernet and Network File System.

2. Data Analysis: For subsequent data analysis the current system also has a number of other functional improvements over its pedecessors including: (1) least-squares Laplacian derivation estimation to reduce volume conduction distortion (Gevins 1989b); (2) digital filters with user-specified characteristics; (3) time series analysis including spectral analysis, Wigner Distributions (Morgan and Gevins 1986), and event-related covariance analysis (Gevins et al. 1987, 1989a; Gevins and Bressler 1988); (4) neural-network-driven pattern recognition to extract optimal or near-optimal subsets of features for recognizing different experimental or clinical categories (Gevins 1980, 1987; Gevins and Morgan 1988); and (5) anatomical modeling to construct 3-D finite element models of the brain and head from MRI scans (Le et al. In Prep.; Brickett et al. In Prep.; Reutter et al. In Prep.). Four on-line, interactive subsystems are used to examine and edit data for residual artifacts (on an individual channel basis if desired), sort data according to stimulus, response or other categories, perform exploratory data analysis, and produce three-dimensional color graphics representations of the brain and head.

MRI Analysis and Modeling Methods

Since commercial MRI analysis packages are not designed for research on functional-anatomical integration and thus lack features essential to our undertaking, we have had to develop our own algorithms and software to produce 3-D brain models suitable for functional localization studies. Visualization software permits construction of 3-D composites of multiple 2-D image planes, as well as 3-D surface rendering based on surface contours. Since generating surface contours manually is laborious and subject to error, we have worked on automating the procedure. We have also automated the alignment of the digitized EEG electrode positions with the scalp surface contours, which is a critical first step in a functional-anatomical analysis. The MRI contour information is used to produce a mathematical finite element model (FEM) of the brain and head suitable for equivalent dipole source localization and scalp EEG deblurring development. Since complex FEM normally run on supercomputers, we made a significant effort to develop FEM algorithms and programs that could run efficiently on a desktop workstation.

EEG-MRI alignment procedure

In order to visualize the brain areas underlying EEG electrodes, a procedure is needed for aligning scalp electrode positions with the MR images. In the procedure we now use, x, y, z translation and x, y, z axis rotations are computed iteratively to align the digitized positions of the EEG electrodes with the MRI data. This is done for each electrode by finding the distance to the closest point on the scalp surface MRI contours and minimizing the mean distance for all electrodes. With MR images that have a 3 mm inter-slice spacing, we usually achieve a mean error distance better than 2 mm. This is more accurate and less subjective than alignment procedures that use skull landmarks such as the nasion and pre-auricular points located visually in the MR images. Figure 6 shows the electrodes displayed schematically on a scalp surface reconstructed from horizontal MRI scalp contours as described below.

3-D Composite MRI displays

Figure 7 shows examples of 3-D composite images taken from a routine clinical MRI exam of a patient with partial seizures. A combination of horizontal, coronal, and sagittal plane images are shown in five different views. Figure 8 shows another composite from the same data and also a partial surface reconstruction done as described below.

Contour extraction and surface rendering

Both the scalp and cortical surface contours in Figures 7 and 8 were traced using an intensity thresholding technique, one of the two image analysis methods we developed to extract scalp and cortical surface contours from MRIs. The first technique uses intensity thresholding, which involves extracting contours along which the image intensity is equal to a defined threshold. This technique is useful for extracting the scalp surface contour which can be discerned easily from the black (approximately zero intensity) background of the image.

The current method of surface rendering has six steps:

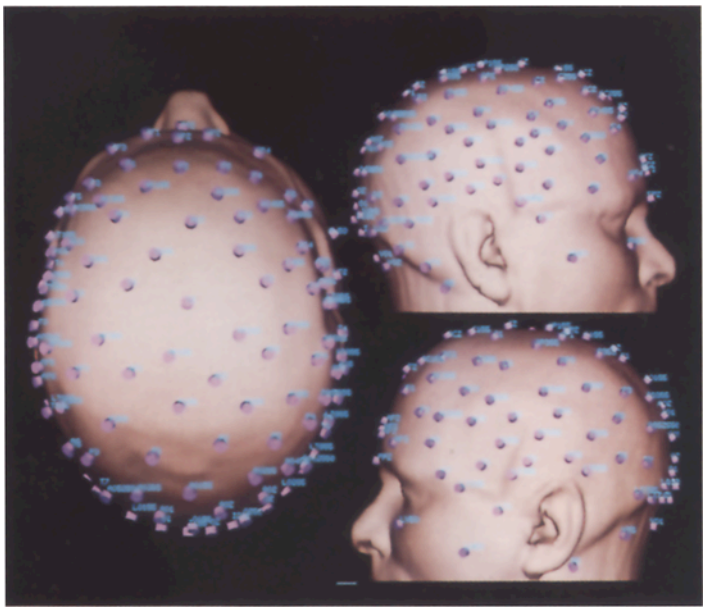

Figure 6: Electrodes schematically displayed as small cylinders, at the actual measured postions, on a 3-D model of the subject's head constructed from his MRIs.

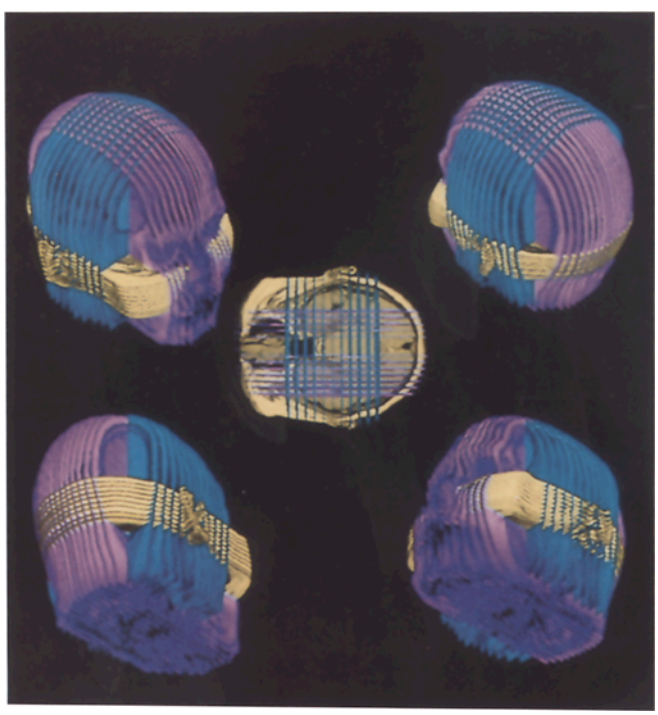

Figure 7: Five views of composite MR images. Horizontal slices are shown in yellow, sagittal in magenta and coronal in blue. For each slice, a closed contour which outlines the scalp is first automatically obtained with a thresholding algorithm. The composites are then drawn for each viewing position by displaying the MR intensity values contained within each contour.

1) for each pair of adjacent contours, find the point on the second contour closest to the first; 2) calculate the two distances from each of these points to the next point on the adjacent contour; 3) make a triangle using the point with the shortest distance, advancing on that contour; 4) repeat steps two and three until all points are exhausted; 5) repeat steps two to four in the reverse direction along the contours; and 6) piece together the "best" result. This was the surface reconstruction method used for Figure 8 showing a surface reconstruction of the cerebral cortex (in yellow), from the same patient as in Figure 7, using the available coronal slices.

The second contour extraction method we have used involves differential intensity analysis. Using this technique, contours that separate image regions with different local average intensities are extracted. Resulting contours pass through the points in the image at which the local average image intensity is changing most rapidly. This technique requires no a priori intensity threshold value, and is useful for extracting the cortical surface contour which has a less well-defined image intensity value throughout an image than the scalp surface contour. The first-order and second-order partial derivatives of the image are estimated using 2-D filters, and these derivatives are used to locate the local maxima in the gradient of the image intensity. Highly computationally efficient filtering techniques have been developed for the estimation of the partial derivatives of the image (Algazi et al. 1989). Figure 9 shows an example of contours corresponding to locations of local maxima in the gradient of the image intensity, which trace sulci.

3-D Cortical surface image model

3-D surface models of the external convexity of the cerebral cortex, such as those of Figure 8, are not sufficient to visualize and computationally model the cortical surface within fissures and sulci. As a result, we developed an algorithm to model cubic volume elements (voxels). The faces of the voxels lie in the horizontal, coronal, and sagittal planes for which MRI data have been obtained. The MRI data are mapped onto the faces of the voxels to obtain a 3-dimensional display of the image data. The image planes used are averaged horizontal planes that lie halfway between the horizontal planes in which MRI data have been acquired, and coronal and sagittal image planes that are synthesized from the acquired horizontal images using linear interpolation. The spacing between image planes is 3 mm, which yields voxels with dimensions of 3 mm by 3 mm by 3 mm. The images have pixel dimensions of approximately 1 mm by 1 mm.

The initial set of voxels is the set bounded by those

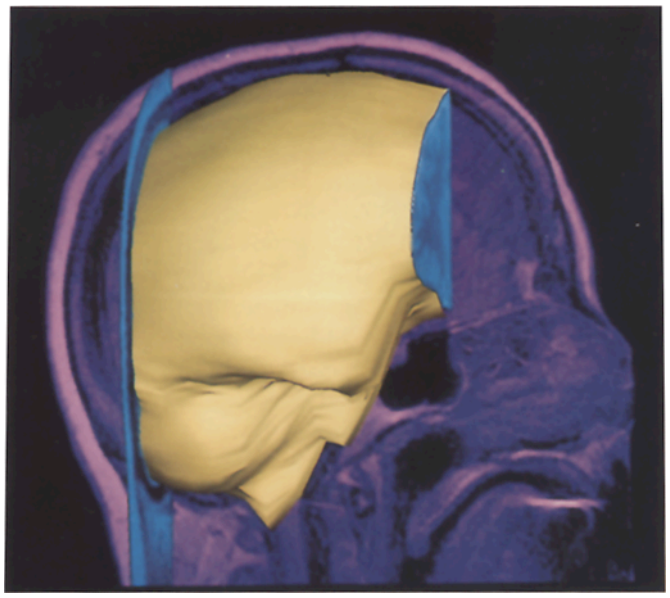

Figure 8: Composite MR images showing a reconstructed cortical surface (in yellow) produced from the automatically traced cortical surface contours. The surface is relatively smooth because it was reconstructed from a standard clinical MRI scan with 5 mm interslice intervals. Also shown are images contained within the scalp contour for one sagittal section (magenta) and one posterior coronal section (blue). The anterior blue image is the coronal data contained within the cortical surface contour.

voxels that lie just inside the cortical surface. To view the MRI data at a slightly deeper level, a mathematical morphology erosion operation is used to remove the boundary layer of voxels, thereby exposing the faces of the voxels that lie one layer deeper. By eroding the model iteratively, anatomical structures can be tracked and 3-dimensional models of the structures can be made (see Figure 12).

Finite element modeling

Maxwell's Equation (Landau et al. 1984; Nunez 1981) states that

$$\nabla \cdot (\sigma \nabla u) + \nabla \cdot J = 0 \qquad in\ \Omega \tag{1}$$

is frequently used to study the electromagnetic field generated by populations of neurons. Here $\sigma(> 0)$ is the conductivity tensor at a point R = (x,y,z) in Ω (e.g., a human head), u is the electric potential at R, and J is the electric current density at R. When Ω represents a human head, the following boundary condition for equation (1) is obtained

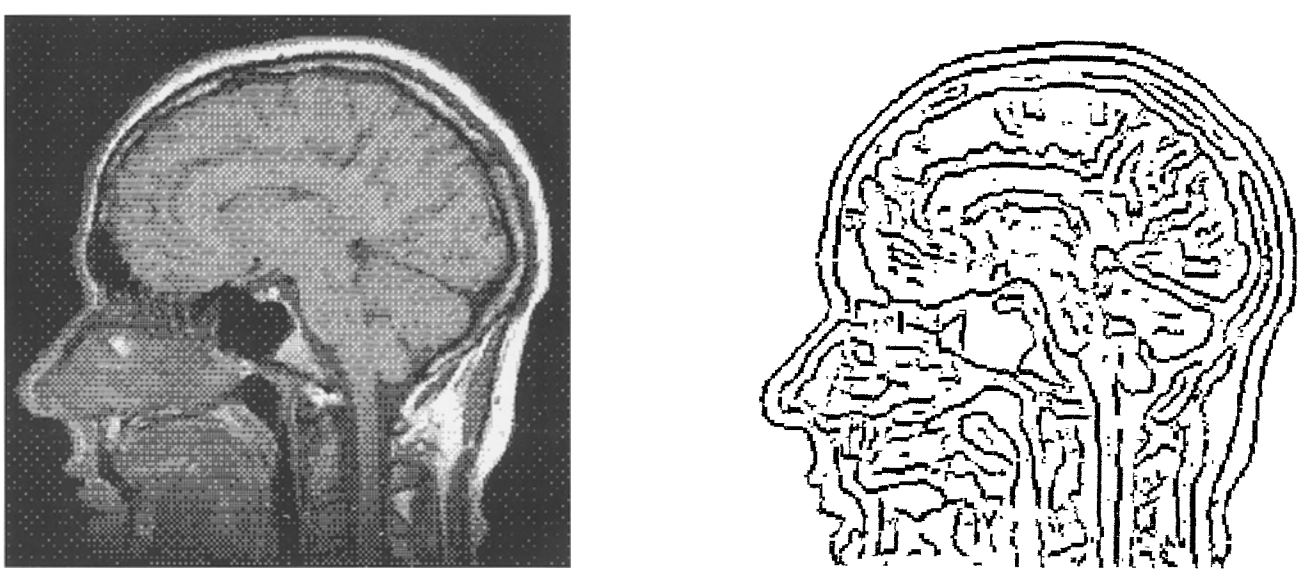

Figure 9: (Left) Midline sagittal MRI obtained with TR=600 and TE=20 ms. (Right) Output of automatic edge-detection software. The lines shown correspond to locations of local maxima in the gradient of the image intensity. These contours pass through the points in the image at which the local average intensity is changing most rapidly.

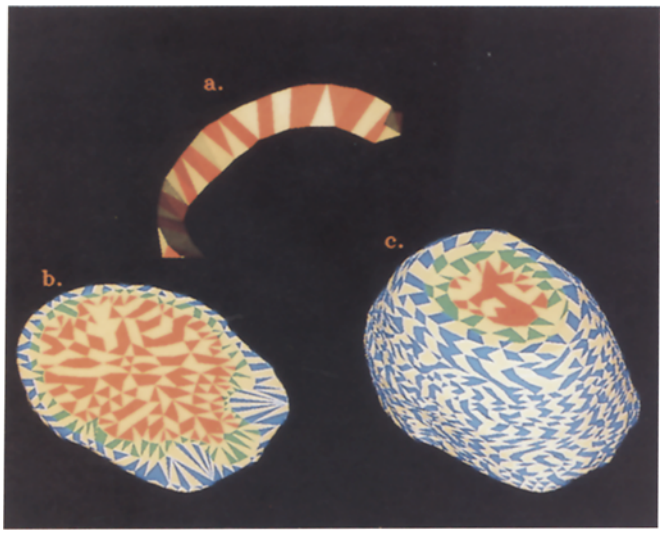

Figure 10: Automated construction of finite elements within brain, skull and scalp volumes, with alternating elements shown in red, green and blue, for the respective tissue type. (a) Tetrahedral elements generated in an outer ring in brain. (b) An entire horizontal slice at the level of the orbits. (c) All slices superimposed except for the topmost horizontal slices.

$$\sigma \nabla u \cdot n = 0 \quad on\ S \tag{2}$$

since electric current does not flow out of the head in the direction normal to the surface. The limited scalp potential measurement specifies another boundary condition.

$$u = U(x, y, z) \quad on\ S_1 \tag{3}$$

Where S_1 is a subsurface of S corresponding to area covered by electrodes. The Finite Element Method (FEM) we developed finds the numerical solution of equation (1) with the boundary condition as specified in equation (2) when the electromagnetic field activities of a head are modeled. Advantages of this approach are: 1) it handles the Dirac Delta Function $\nabla \bullet J$ smoothly by transforming equation (1) into a variational form when J represents a dipole-like kind of source; 2) it allows us to model the complicated geometries of different tissues within the head by generating finite elements using contours on pairs of adjacent MR images; and 3) it produces a sparse matrix in which many entries are zeroes. We developed efficient sparse matrix techniques (Le et al. in prep.) that can solve Maxwell's equation at 10,087 FEM nodes in about 100 min on a SUN Sparc-1 workstation (12 MIPS) with 8MB of memory (Figure 10).

We can use this analysis to localize single equivalent dipole sources of recorded scalp potentials, or obtain the potential distribution within the whole head given the localized source. To do this, we choose a specific function J and solve the corresponding potential distribution u using FEM such that the difference between u on S_1 and $U(x,y,z)$ defined on S_1 is minimized using an iterative process. Another use of FEM, in which the current distribution on the surface of the brain is estimated from scalp recordings, is described in the next section.

Towards Functional-Anatomical Integration

Spatial filters to reduce blur distortion

Electrical currents generated by sources in the brain are volume conducted through brain, cerebrospinal fluid, skull and scalp to the recording electrodes. Because of this, potentials due to a localized source are spread over a considerable area of scalp and the potential measured at a scalp site represents the summation of signals from many sources over much of the brain. Using a 4-shell spherical head model, we have estimated the "point spread" for a radial dipole in the cortex to be about 2.5 cm (Doyle and Gevins, Submitted). The "simplest" way to reduce this distortion is to take the Laplacian in two dimensions about each electrode. Details of this method, however, are less straightforward than they might seem, as discussed below. Another improvement in distortion is possible, in principle, by using a Finite Element Method and estimates of the conductivity properties of the tissue between brain and scalp surface to estimate the potentials which would actually be recorded on the surface of the brain.

1. Laplacian operator: A local Laplacian operator produces an appreciable reduction of the spatial low-pass distortion caused by the blurring effects of the skull. Poisson's equation states that the Laplacian of the potential is proportional to the local density of current sources. An estimate of the average Laplacian over a volume of scalp surrounding a given electrode will then be proportional to the net current leaving that volume. The 2-D Laplacian in the plane of the scalp is proportional to the net current through the edges of the volume. Since there are no current sources in the volume, this net current is equal to the local density of current flow up through the skull (local current source density or CSD) (Hjorth 1975). It should be noted that this term does not refer to neuronal sources, but only to local current emerging from the skull.

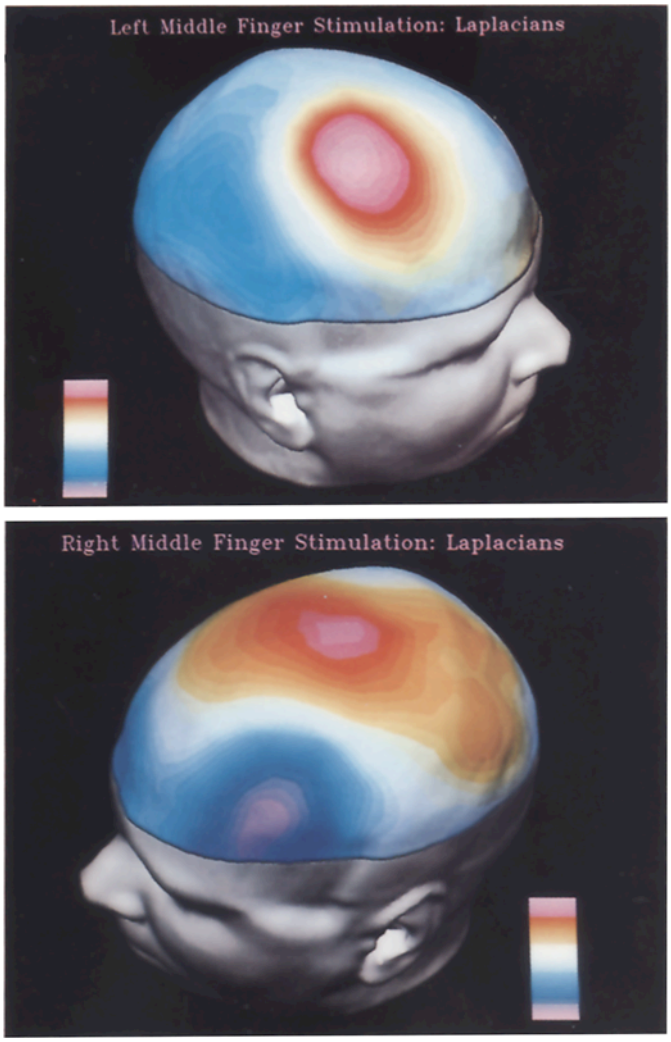

Figure 11: Laplacian of 124-channel evoked potentials evoked by 15-Hz stimulation of the middle finger on left (top) and right (middle) hands of this subject mapped onto his own MRI-derived scalp surface. The map for the right index finger is shown in the bottom panel. Color scale shows zero as white and the maximum as magenta. (Bottom panel on p. 64.)

This transform has a localizing effect since it is relatively insensitive to sources beyond the proximal electrodes. It also has the advantage of being independent of reference electrode site. The usual implementation (Hjorth 1980; Thickbroom et al. 1984) estimates the Laplacian operator at a given electrode as an average of the directional derivatives from each surrounding electrode to the given electrode. This quantity is proportional to a second-difference estimate of the Laplacian for a "rosette" of electrodes uniformly surrounding the given electrode with the factor of proportionality being a geometrical factor (the electrode separation squared), but departs from the same proportionality as the configuration of electrodes departs from the symmetrical, notably when all the proximal electrodes are on one side of the given electrode. We have improved upon the conventional method of Hjorth (1975), by using actual measured interelectrode distances, and by forming an optimal least squares estimate of the signal at each electrode (Gevins 1989b). We are currently testing a further improved version which accounts for the actual 3-D shape of the head and does a spline interpolation of the potentials.

2. Finite Element Method deblurring in a realistic head model: Since an "image" of the potential distribution over local cortical areas is highly desirable, spatial deblurring methods can be used to reduce volume conduction and increase spatial resolution. One method of doing this without introducing an arbitrary model of the actual number and location of sources is to use finite element methods to represent the true geometry of cortex, cerebrospinal fluid, skull and scalp, and to model the potential activity described by Maxwell's equations in the scalp and skull layers. This operation could be performed without imposing an arbitrary source model because, regardless of where they are generated in the brain, potentials recorded at the scalp must arise from volume conduction from the cortical surface through the skull and scalp. While we expect this method to produce an estimate of the current distribution at the cortical surface, it does not identify the number, position, or orientations of sources. (For instance, the skull currents resulting from a tangential dipole source in the cortex might still be difficult to distinguish from that caused by two radial dipole sources.)

For this application, the region of interest is limited to the scalp volume and skull volume. The difference between the inner surface of the skull and the outer convexity of the cortical surface is assumed to be small enough to be neglected. We also assume that the potential activity in the region of interest is described by Maxwell's equation, that the boundary condition on the air-scalp surface is stated by equation (2), i.e., current cannot flow out of the scalp, and that the boundary condition on the cortical surface is stated by the following equation (4) which describes the cortical surface potentials.

$$u = G(x, y, z) \quad on \ S_2 \tag{4}$$

We also assume that there is no generating source within the scalp or skull which means the function J in equation (1) is zero. Although of course there is no general solution to the "inverse problem," because of the assumed boundary conditions there is a unique solution of equation (1), which may be obtained as follows. Applying the Finite Element Method to equation (1) with boundary conditions in (2) and (4), the following matrix vector relation is obtained (Le et al. in prep.)

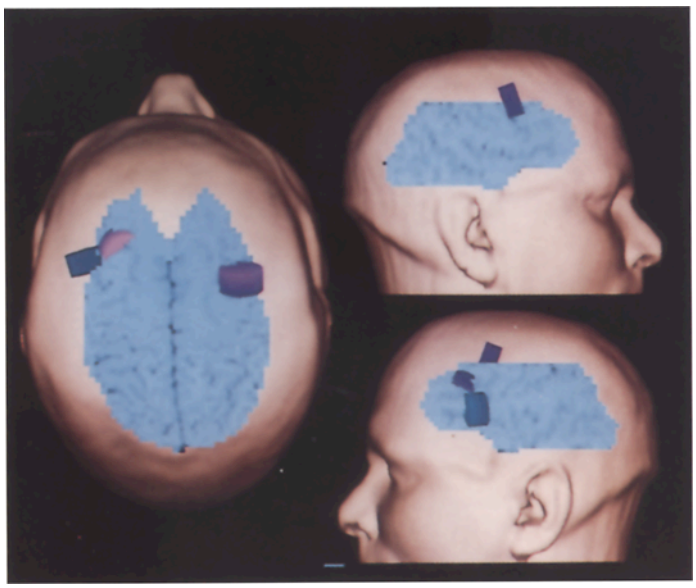

Figure 12: Integration of EEG and MRI data as a step towards anatomical-functional localization. The data shown in Figure 11 were used to compute best-fitting single equivalent dipoles using a three-sphere head model. The figure shows top, left and right views of the scalp surface reconstructed from horizontal MR images. The voxel brain model shown in light blue corresponds to four stages of erosion of 3 mm layers, hence its shrunken appearance. The dipole for right index finger stimulation (dark blue) is located most left-laterally. The middle finger dipoles (purple) are located appropriately in contralateral hemispheres.

$$A\,u = f \tag{5}$$

Here **u** is a vector of dimension n, which is a numerical approximation to the analytical potential distribution function u in equation (1). The value of n corresponds to the total number of vertices on all the finite elements in the region of interest. Since we are assuming that no generating sources are present in the skull and scalp, $J \equiv 0$ and therefore $\mathbf{f} = \mathbf{0}$. We then decompose u into three sets, the potentials which correspond to the electrodes on the scalp, the potentials which correspond to the cortical surface, and the potentials in the rest of the region, and denote them by $\mathbf{u_1}$, $\mathbf{u_3}$ and $\mathbf{u_2}$ respectively. If we decompose the matrix **A** correspondingly, then quation (5) becomes:

$$\begin{pmatrix} A_{11} & A_{12} & A_{13} \\ A_{21} & A_{22} & A_{23} \\ A_{31} & A_{32} & A_{33} \end{pmatrix} \begin{pmatrix} u_1 \\ u_2 \\ u_3 \end{pmatrix} = 0$$

Solving $\mathbf{u_1}$ with respect to $\mathbf{u_3}$, we get

$$(A_{11} - A_{12} A_{22}^{-1} A_{21})\, u_1 = (A_{12} A_{22}^{-1} A_{23} - A_{13})\, u_3 \tag{6}$$

and solving $\mathbf{u_3}$ with respect to $\mathbf{u_1}$, we get

$$(A_{22}^{-1} A_{23})\, u_3 = (A_{32} A_{22}^{-1} A_{21} - A_{31})\, u_1 \tag{7}$$

For a given G_k, u_3^k is known. Then u_1^k can be computed via equation (6) and the residual is calculated from u_1^k and $U(x,y,z)$ which correspond to the predicted and measured potentials, respectively.

3. Estimating conductivities and evaluating deblurring method: Up to now, estimates of conductivity for the scalp, skull, CSF and brain have been published (Geddes and Baker 1967; Hosek 1970). We have attempted to estimate skull conductivity by injecting small currents at one electrode and recording at the others for many combinations of stimulating and recording electrodes (Gevins and Doyle, Unpublished data). This has failed, however, because of the obvious shunting effect of the scalp. We are currently working on a more direct approach that does not involve applying external stimuli but rather uses known natural sources of activity. We are evaluating the method by comparing deblurred scalp data with subdural grid data recorded from the same patient.

Equivalent dipole modeling of somatosensory stimulation

We are just beginning to apply the methods described above to functional-anatomical localization. The first application was to perform equivalent dipole modeling of somatosensory stimulation. For this purpose, the middle fingers of the left and right hands, and the right index finger were each electrically stimulated at 15 Hz for three 100-second intervals. Artifact-free epochs of 0.533 seconds were averaged, and Fourier-transformed real and imaginary components of the 15-Hz response were averaged over each 100-second run. Data for each of the

three runs were then combined for each finger for calculation of the "canonical" phase, i.e., that phase angle onto which the projections of all the phasors yielded the greatest squared amplitude. These steady-state amplitude measures were used to construct topographical maps and for least-squares fitting of equivalent current dipoles. Preliminary results for the first subject (Figure 11) show topographical maps of the Laplacian of the evoked responses to stimulation of the left and right middle fingers. (Each map is scaled separately. Amplitude of the right finger response is approximately one half that of the left.) Figure 12 presents the result of fitting single equivalent dipoles to these data and also the result for the right middle finger. Dipoles are shown with respect to the scalp surface and eroded brain model described above. Each dipole is represented as a disk with it's center on the dipole location, and axis in the dipole direction. Each dipole appears in the contralateral hemisphere, and the dipole for the forefinger is located slightly more lateral than that for the middle finger, consistent with the known locations of the sensory projection areas and other physiological source localization results (Luders et al. 1986; Wood et al. 1985).

Conclusion

There is no doubt that much useful information lies hidden in the EEG. We are optimistic about advancing our technology to mine this hidden information, and to further our investigations of the neural substrate of human higher cognitive brain functions.

References

Algazi, V.R., Reutter, B.W., van Warmerdam, W.L.G and Liu, C.C. Three-dimensional image analysis and display by space-scale matching of cross sections. J. Opt. Soc. Am., 1989: 6, 890-899.

Brickett, P. and Gevins, A.S. Retinotopic source localization of 15-Hz pattern-reversal evoked potentials, in preapration.

Doyle, J.C. and Gevins, A.S. Technical Note: Spatial filters for event-related brain potentials. EEG clin. Neurophysiol., submitted.

Geddes, L.A. and Baker, L.E. The specific resistance of biological material - a compendium of data for the biomedical engineer and physiologist. Med. Biol. Engr., 1967: 5, 271-293.

Gevins, A.S. Application of pattern recognition to brain electrical potentials. IEEE Trans. Pattern Ana. Mach. Intell., 1980: PAM-12, 383-404.

Gevins, A.S. Analysis of the electromagnetic signals of the human brain: Milestones, obstacles and goals. IEEE Trans. Biomed. Enginr., 1984: BME12(31), 833-850.

Gevins, A.S. Statistical pattern recognition. In A. Gevins and A. Remond (Eds.), Methods of Analysis of Brain Electrical and Magnetic Signals: Handbook of Electroencephalography and Clinical Neurophysiology (Vol. 1), Amsterdam, Elsevier, 1987.

Gevins, A.S. Recent advances in neurocognitive pattern analysis. In: E. Basar (Ed.), Dynamics of Sensory and Cognitive Processing of the Brain. Heidelberg, Springer-Verlag, 1988: 88-102.

Gevins, A.S. Signs of model making by the human brain. In: E. Basar and T. Bullock (Eds.), Dynamics of Sensory and Cognitive Processing by the Brain. Springer-Verlag, 1989a: 408-419.

Gevins, A.S. Dynamic Functional Topography, Brain Topography, 1989b: 2(1), 37-56.

Gevins, A.S. and Bressler, S.L. Functional topography of the human brain. In: G. Pfurtscheller (Ed.), Functional Brain Imaging. Hans Huber Publishers, Bern, 1988: 99-116.

Gevins, A.S. and Morgan, N.H. Applications of neural-network (NN) signal processing in brain research. IEEE ASSP Trans., 1988: 7, 1152-1161.

Gevins, A.S. and Remond, A. (Eds.) Methods of Analysis of Brain Electrical and Magnetic Signals. Handbook of Electroencephalography and Clinical Neurophysiology, Vol.1. Amsterdam, Elsevier, 1987.

Gevins, A.S. and Yeager, C.L. EEG spectral analysis in real time. DECUS Proc. Computers in Medicine, 3 1972: 4, 71-74.

Gevins, A.S. Yeager, C.L., Diamond, S.L., Spire, J.P., Zeitlin, G.M. and Gevins, A.H. Automated analysis of the electrical activity of the human brain (EEG): A progress report. IEEE Proc., 1975: 63(10), 1382-1399.

Gevins, A.S. Doyle, J.C., Cutillo, B.A., Schaffer, R.F., Tannehill, R.L., Ghannam, J.H., Gilcrease, V.A. and Yeager, C.L. Electrical potentials in human brain during cognition: New method reveals dynamic patterns of correlation. Science, 213, 1981: 918-922.

Gevins, A.S., Cutillo, B.A., Bressler, S.L., Morgan, N.H., White, R.M., Greer, D.S., Illes, J. Event-related covariances during a bimanual visuomotor task, Part I: Methods and analysis of stimulus-and response-locked data. EEG clin. Neurophysiol., 1989: 74(1), 58-75.

Hjorth, B. An on-line transformation of EEG scalp potentials into orthogonal source derivations Electroenceph. clin. Neurophysiol., 1975: 39, 526-530.

Hjorth, B. Source derivation simplifies topographical EEG interpretation. Amer. J. EEG Technol., 1980: 20, 121-132.

Hosek, A.R. An experimental and theoretical analysis of effects of volume conduction in a nonhomogeneous medium on scalp and cortical potentials generated in the brain. Doctoral dissertation, Marquette Univ. Biomed. Engr., 1970.

Jasper, H. H. The ten-twenty electrode system of the international federation. Electroenceph. clin. Neurophysiol., 1958: 10, 371-375.

Landau, L.D, Lifshitz, E.M. and Pitaevskii, Electrodynamics of Continuous Media. New York: Pergammon, 1984.

Le, J., Brickett, P. Surkis, A. and Gevins, A.S. Finite element modeling of Maxwell's equations in a realistic human head, in preparation.

Lopes da Silva, F., Storm van Leeuwen W., Remond, A. (Eds.), Handbook of Electroencephalography and Clinical

Neurophysiology, Vol. 2: Clinical Applications of Computer Analysis of EEG and other Neurophysiological Signals. Amsterdam, Elsevier, 1986.

Luders, H., Dinner, D.S., Lesser, R.P. and Morris, H.H. Evoked potentials in cortical localization. J. Clin. Neurophysiol., 1986: 3, 75-84.

Nunez, P. Electric Fields of the Brain. New York: Oxford, 1981.

Reutter, B.W., Brickett, P., Gevins, A.S. Algorithms for analysis of Magnetic Resonance Images, in preparation.

Thickbroom, G., Mastaglia, F., Carroll, W. and Davies, H. Source derivation: application to topographic mapping of visual evoked potentials. J. Electroenceph. clin. Neurophysiol., 1984: 59, 279-285.

Wood, C., Cohen, D., Cuffin, B.N., Yarita, M. and Allison, T. Electrical sources in human somatosensory cortex: Identification by combined magnetic and potential recordings. Science, 1985: 227, 1051-1053.

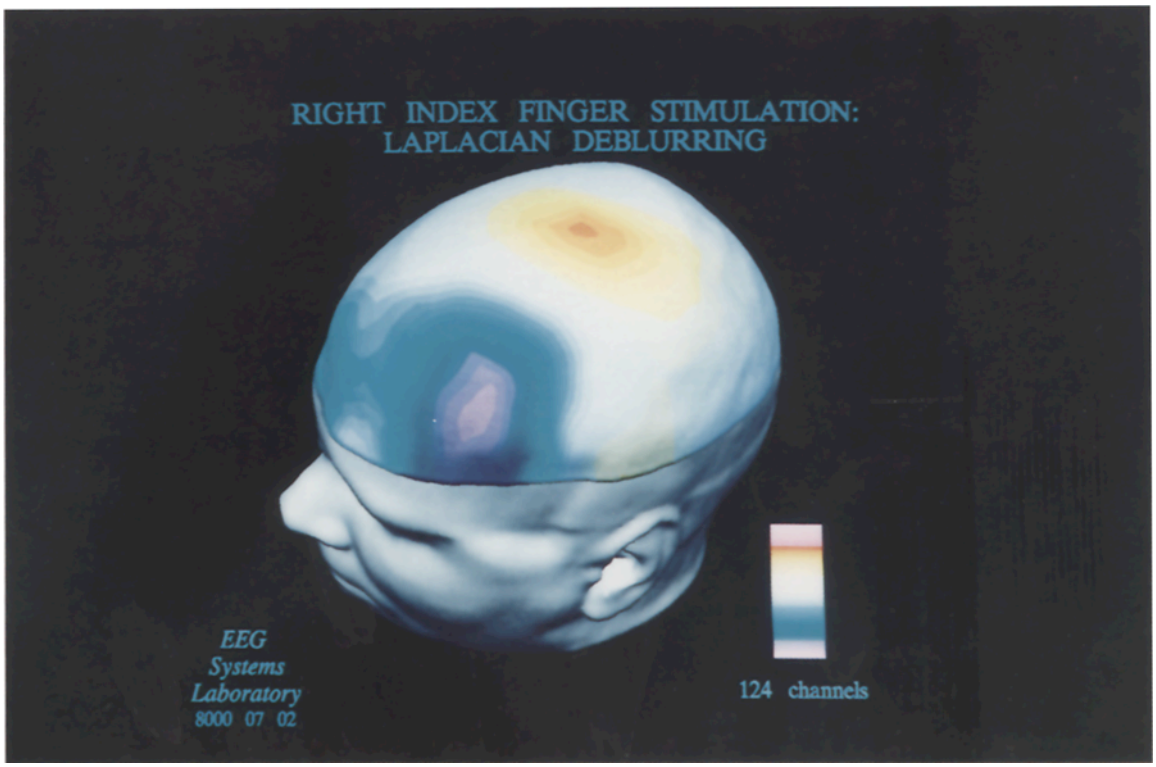

Figure 11, Bottom panel.